ATMOSPHERIC ENVIRONMENT: X 24 (2024) 100298

Contents lists available at ScienceDirect

Atmospheric Environment: X

journal homepage: www.journals.elsevier.com/atmospheric-environment-x

Regional and seasonal impact of hydrogen propulsion systems on potential contrail cirrus cover

Stefan Kaufmann [a,*], Rebecca Dischl [a,b], Christiane Voigt [a,b]

[a] Deutsches Zentrum für Luft- und Raumfahrt, Insitut für Physik der Atmosphäre, Oberpfaffenhofen, Germany
[b] Johannes Gutenberg University Mainz, Mainz, Germany

ARTICLE INFO

Keywords:
Hydrogen propulsion
Contrail cirrus

ABSTRACT

The decarbonization of air transportation requires novel propulsion concepts in order to replace fossil kerosene powered gas turbines. Within various options, H_2 based propulsion is one of the most promising candidates, at least for regional and short haul routes. However, despite the potential to reduce CO_2 emissions to zero, those aircraft can still have a significant climate impact due to increased contrail formation caused by higher water emission when using H_2 as a propellant. In order to understand potential changes in the climate impact of H_2 powered air traffic, it is crucial to evaluate how the potential for contrail formation and the potential contrail cirrus cover would change under representative atmospheric conditions. To this end, we developed a tool which uses several years of meteorological reanalysis data (ERA-5 and MERRA-2) in combination with contrail formation conditions adjusted to H_2 gas turbine and H_2 Fuel Cell propulsion in order to investigate their regional and seasonal variation. Contrail formation conditions for three different propulsion settings (kerosene gas turbine, H_2 gas turbine and H_2 fuel cell) are calculated to obtain global statistics of potential contrail cover and potential contrail cirrus cover over 12 years. For H_2 based propulsion contrails are more likely to form due to the increased water vapor emission. However, this does not necessarily translate into the climatically relevant potential for contrail cirrus formation. Focusing on three hot spots of regional air traffic, we find that the difference between kerosene and H_2 scenarios has a strong systematic dependency on season, altitude and latitude. Maximum differences in potential contrail cirrus cover are found in the transition region from typically no-contrail to contrail forming conditions at a potential contrail cover around 50%. In contrast, less to no difference in potential contrail cirrus cover is found at very high (close to 100%) or rather low potential contrail cover. This study demonstrates, that the question whether H_2 powered air traffic produces more climate relevant contrail cirrus can not be parameterized by a simple factor but rather strongly depends on the propulsion type, season, region and flight altitude.

1. Introduction

The transition to a global air transportation sector with substantially reduced climate impact until 2050 as aimed e.g. in the EU Green Deal (European Comission, 2024) will very likely include hydrogen as propellant to either directly operate gas turbines or produce electric energy to power propulsion systems. Major aircraft and engine manufacturers aim for a realization of commercial hydrogen powered aircraft in the time frame 2035 to 2050 (Airbus, 2024). Despite technical challenges like the high energy demand for hydrogen production and storage and the lower volume specific energy density compared to fossil kerosene, it could be seen superior compared to other technologies like storing electric energy in batteries, at least for the short to medium range segment (Adler and Martins, 2023). Considering only the emissions during flight, hydrogen would obviously reduce CO_2 emissions to zero immediately. However, the climate impact of aviation is not only caused by CO_2 emissions but also significantly by NO_x and contrail cirrus (Lee et al., 2021).The radiative forcing of water vapor, contrail cirrus and leaking H_2 (Warwick et al., 2023) is expected to counteract the reduced CO_2 emissions when partially replacing aircraft fleets by hydrogen powered airplanes since propulsion by hydrogen implies the emission of more water vapor which, in comparison to kerosene powered aircraft, can lead to contrail formation at warmer temperatures and lower flight altitudes (e.g. Schumann (1996); Gierens (2021); Grewe et al. (2017)).

* Corresponding author.
E-mail address: Stefan.Kaufmann@dlr.de (S. Kaufmann).

https://doi.org/10.1016/j.aeaoa.2024.100298
Received 10 May 2024; Received in revised form 27 September 2024; Accepted 1 October 2024
Available online 5 October 2024

The climate impact from contrails is much harder to assess than that of CO_2 since it depends on various factors like meteorological conditions determining contrail optical depth, contrail lifetime, and surrounding natural clouds (e.g. Bock and Burkhardt (2019)). Furthermore, its quantification depends on the climate metric which is used to compare both effects (Borella et al., 2024). Ponater et al. (2006) calculated different transition scenarios to H_2 powered air traffic and found a small decrease in contrail RF and a slight decrease in surface temperature change(see also Marquart et al. (2005)).

Microphysical and thus radiative properties of contrails from hydrogen propulsion are likely to differ from contrails produced by kerosene gas turbines (Adler and Martins, 2023; Grewe et al., 2017). The main reasons for this difference is the absence of soot emissions which are the dominant nucleus for initial activation of liquid droplets, which subsequently freeze into contrail ice particles. Both experimental and modelling studies have shown that ice particle number concentrations in contrails are reduced with reduced soot emissions (Voigt et al., 2021; Bier et al., 2024). The latter study also showed that the high potential supersaturation with respect to water in the plume can lead to activation of either alternative emitted aerosol species or entrained ambient aerosol that could finally grow into ice.

In this study we apply a statistical approach evaluating the atmospheric conditions in terms of contrail formation and potential persistent contrail cirrus from hydrogen fuel cell and gas turbine engines in comparison to aircraft with traditional kerosene powered gas turbines. Comparable to Sausen R. et al. (1998) and more recently Hofer et al. (2024a), we process 12 years of meteorological reanalysis data of temperature and relative humidity from ERA-5 or MERRA-2. Therefore, we use the CoStat tool, an updated version of the work by Dischl et al. (2022). Here, the threshold temperatures for contrail formation from H_2 fuel cells and H_2 gas turbines are additionally implemented as calculated by Gierens (2021). As in Dischl et al. (2022), the output quantity is potential contrail and contrail cirrus cover for aircraft with defined engine characteristics. As such the tool does not model the climate impact of contrails but is a useful tool for sensitivity studies of the effect of different propulsion systems on potential contrail and contrail cirrus cover. Thus, it can be seen as first part of the chain which is embedded in a large suite of modelling approaches aiming to investigate the contrail effect from future air transportation. Those approaches start with small scale LES simulations (Unterstrasser, 2016), comprise computing the radiative impact of single contrails as done in CoCip (Schumann, 2012) and pycontrails (Teoh et al., 2022a) and range up to global climate models which calculate global contrail radiative forcing (e.g. Burkhardt et al. (2018); Bock and Burkhardt (2019)).

After a short description of the tool and the implementation of the H_2 based propulsion settings, the manuscript describes the main differences of the potential to form contrails (potential contrail cover) and the potential contrail cirrus cover. The main scientific question for this work is, how the potential contrail cirrus cover would change if current aircraft are replaced by a hypothetical H_2 powered fleet. In a global view, we analyze the influence of propulsion type, season and altitude on the potential for contrail formation and on the potential contrail cirrus cover. Since the transition from kerosene to H_2 propulsion is likely to happen first in the regional and short haul segment, we focus on three global hot spots with high regional air traffic density, namely the US, Central Europe and Southeast Asia. We show, that the difference in potential contrail cirrus cover between aircraft with H_2 propulsion and regular kerosene turbines varies strongly with altitude and season, which potentially offers operational mitigation of additional contrail cirrus from hydrogen propulsion.

2. Methods

2.1. Description of the CoStat tool

CoStat is a python based tool, that provides statistics on potential contrail and potential contrail cirrus cover for different propulsion concepts using temperature and relative humidity fields from reanalysis models. It is based on the tool described in Dischl et al. (2022) with enhanced data input capabilities (global datasets from ERA-5 and MERRA-2) and H_2-based propulsion types. The architecture of the tool is shown in Fig. 1. As described in detail in Dischl et al. (2022) we calculate the threshold temperatures for contrail formation using the Schmidt-Appleman Criterion (Schumann, 1996) for kerosene gas turbine (Kerosene GT), for H_2 fuel cell (H2 FC) and H_2 gas turbine (H2 GT) following Gierens (2021) (described in 2.2). In a first step, these threshold conditions are used to evaluate the frequency of potential contrail cover for temperature and RH reanalysis fields for a given time period in the year using either ERA-5 (Hersbach et al., 2018) or MERRA-2 (Global Modeling and Assimilation Office, 2015) reanalysis data (details in section 2.3). The potential contrail cover is the frequency of whether a contrail would have formed if an airplane with the specific propulsion parameters flew through that region for a single grid point for the analyzed time period. Since the condensed water droplets formed in the engine exhaust freeze at temperatures below 235K (Schumann (1996), Koop et al. (2000)), we apply an additional temperature threshold of $T_{thres} < 235K$. The consequences of this threshold condition are discussed in Section 2.2. Since from the climate impact point-of-view only longer lived contrail have a significant impact on the atmospheres radiation budget (Burkhardt et al., 2018; Teoh et al., 2022a), in a second step, we apply a RH threshold in order to determine regions with potential contrail cirrus cover. Following the idea of previous studies to correct the underestimation of RHi in ERA around saturation (Hofer et al. (2024b); Teoh et al. (2022a)), we choose a default threshold of RHi $> 95\%$ to calculate the potential contrail cirrus cover. As resulting product, the CoStat tool provides maps with spatial distributions for potential contrail and contrail cirrus cover for the selected time period (e.g. one month of the year) with a statistical distribution over an adjustable amount of years. As a reasonable compromise between sufficient statistics and computation time, we choose a default statistical period over 12 years from years 2010–2021. The tool provides two different types of output files, one being the overall mean of potential contrail and contrail cirrus cover (used for the maps plot) and the second being year-by-year data of the same quantities for the selected period to address inter-annual differences. In addition to the maps of potential contrail and contrail cirrus covers, the tool computes mean values and spatial percentiles for selected regions of interest within the reanalysis

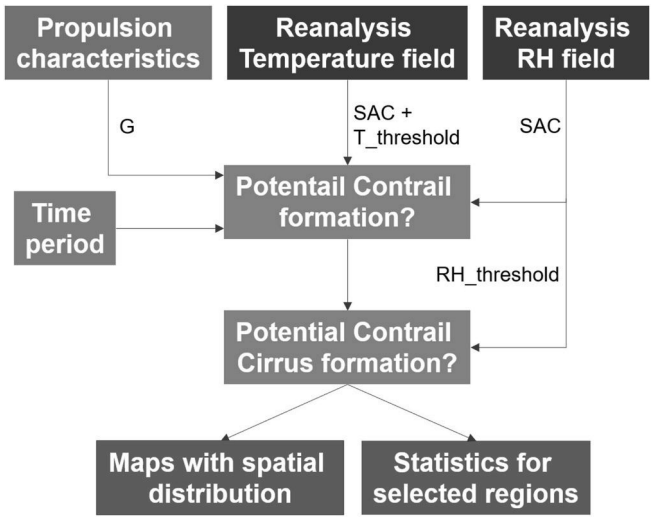

Fig. 1. Flowchart of the CoStat tool. The Potential Contrail Cover is calculated from Temperature and RH reanalysis fields using the slope of the mixing line from the propulsion characteristics input. In the next step, the RHi threshold determines Potential Contrail Cirrus regions.

data sets in order to enable the quantitative evaluation of the effect of e. g. different propulsion types and parameters, regions, seasons and altitudes.

2.2. Implementation of propulsion types

In order to account for the different emission characteristics for H_2 based propulsion systems the calculation of the Schmidt-Appleman criterion needs to be adapted. Particularly relevant for contrail formation are the changes in water vapor emission index, combustion heat or reaction enthalpy and efficiency. One approach to adapt the Schmidt-Appleman theory to H_2 gas turbine and fuel cell powered propulsion is presented by Gierens (2021). It follows the same idea as applied for kerosene gas turbine propulsion, where the slope of the isobaric mixing line in the phase diagram is determined by the difference in water vapor partial pressure of the plume at the exhaust point e_p minus the water vapor partial pressure in the ambient atmosphere e_a divided by the temperature difference between plume and ambient conditions. Following Schumann (1996), this ratio can be expressed via engine specific parameters and pressure:

$$G_{KERO} = \frac{e_p - e_a}{T_p - T_a} = \frac{EI_{H2O} c_p p_a}{\epsilon Q (1-\eta)}, \tag{1}$$

where $c_p \approx 1004\ \mathrm{J\,kg^{-1}\,K^{-1}}$ is the specific heat capacity of air at constant pressure, EI_{H_2O} is the water vapor emission index in kg H_2O per kg fuel burnt (depending on the H/C ratio of the fuel used), p_a is the ambient pressure, ϵ is the molar mass ratio of water and air, Q the specific energy content of the fuel and η the overall propulsion efficiency. In the following we use a default value of H/C = 14.2 mass% for the hydrogen content of the kerosene, which is on the higher end of current kerosene composition and thus representing a rather clean kerosene to compare with future hydrogen based systems. The default parameters used for the calculation of G factors are given in Table 1.

The formulation of the slope of the mixing line for an H_2 powered gas turbine is similar to the kerosene powered gas turbine (Eq. (2), Gierens (2021)). The only difference is the higher water vapor emission index and the higher reaction enthalpy $|\Delta h|$ (Table 1) resulting in a G factor being around 2.5 times higher than for kerosene for the default parameters used here. Qualitatively, this means that the higher water vapor emission overcompensates the higher energy content of the fuel leading to contrail formation at higher threshold temperatures for the H_2 compared to the kerosene gas turbine.

$$G_{H2GT} = \frac{EI_{H2O} c_p p_a}{\epsilon (1-\eta) |\Delta h|} \tag{2}$$

The approach to calculate contrail formation thresholds for fuel cell powered airplanes differs to the traditional gas turbines since the fuel cell likely powers electrical motors and its exhaust is thus decoupled from the actual propulsion system. In consequence the implementation of fuel cells as energy provider opens a much wider parameter space in terms of emission conditions relative to the gas turbines. Nevertheless, the assumption of a direct release of the hot and humid fuel cell exhaust into the atmosphere allows a formulation of the G-factor which qualitatively resembles the ones for gas turbines (Gierens, 2021):

$$G_{H2FC} = \frac{\overline{c_p} p_a}{(1-\eta_e \eta_0) |\Delta h|'} \tag{3}$$

Since all parameters are given as molar fractions here, the water vapor emission index is unity and doesn't explicitly appear. $\overline{c_p}$ is a mean molar heat capacity assuming a stochiometric gas mixture in the fuel cell. $|\Delta h|'$ is the molar enthalpy of the reaction of H_2 and O_2 to H_2O. η_0 is the basic efficiency of the fuel cell given by the ratio between Gibbs energy Δg and enthalpy Δh. Finally, Gierens (2021) defines the electrical efficiency η_e as ratio between the actual operating voltage U of the fuel cell and the electromotive force which equals 1.19 V if water is released as vapor. In this study we choose a default value of U = 0.7 V as estimation for operating conditions under electrical load (Jiang and Qingfeng, 2021). However, contrail formation in typical atmospheric conditions is not very sensitive to the exact number of the operating voltage, in most cases a contrail will form for any reasonable values of U. This approach does not consider any technical alterations of the fuel cell exhaust like heat recuperation or water separation. While heat exchange techniques would just further increase contrail threshold temperatures, the effect of water separation systems is difficult to predict without knowledge of the exact realization. Condensation of exhaust water and subsequent release of liquid droplets could e.g. lead to few but very large ice crystals which sediment very fast. Such a contrail would have a much smaller climate impact compared to gas turbine contrails.

To illustrate the difference between the contrail formation characteristics of the different propulsion types, Fig. 2 shows the phase diagram and the three mixing lines for the default engine parameters as given in Table 1 for ambient conditions of $T_a = 227$ K and $RHi_a = 90\%$. As soon as one of the mixing lines has a section above the dotted liquid saturation curve, liquid droplets form in the cooling exhaust and subsequently freeze to form a contrail. For the specific parameters shown in Fig. 2, both H2 FC (blue) and H2 GT (red) will thus form a contrail while the Kerosene GT is right at threshold conditions for contrail formation. In order to visualize the decision process implemented in CoStat, the critical mixing line for the fuel cell configuration is shown (purple line), defined as the tangent line with the slope G_{H2FC} at the liquid saturation curve. The critical mixing line determines two relevant threshold temperatures for the contrail formation decision in the CoStat algorithm: (1) T_{MIN} at the intersection between critical mixing line and x-axis ($p_{H_2O} = 0$

Table 1
Default propulsion parameters for SAC calculation.

	Kerosene GT	H2 GT		H2 FC
EI_{H_2O} [kg/kg]	1.273	9	EI_{H_2O} [mol/mol]	1
c_p [J kg^{-1} K^{-1}]	1004	1004	$\overline{c_p}$ [J mol^{-1} K^{-1}]	30.6
η	0.35	0.35	η_e	0.588
ϵ	0.622	0.622	η_0	0.945
Q, $\lvert\Delta h\rvert$ [10^6 J kg^{-1}]	43.2	120.9	$\lvert\Delta h\rvert'$ [10^3 J mol^{-1}]	241.82

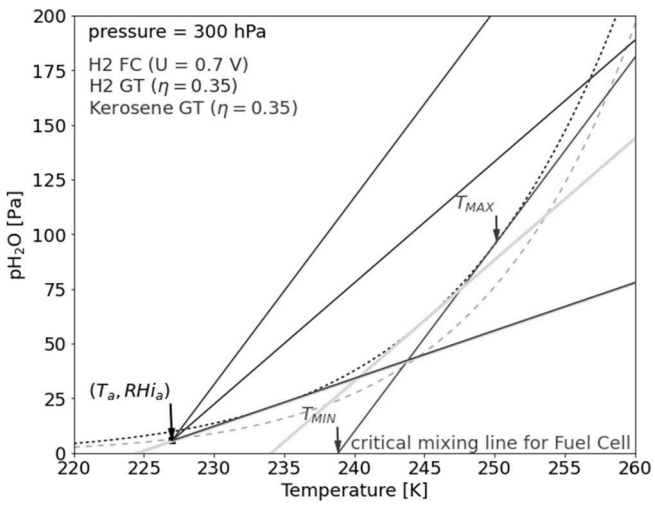

Fig. 2. Phase diagram with mixing lines for the three different propulsion types. The dashed and dotted lines are ice and water saturation, respectively. The blue, red and black lines are actual mixing lines for a given atmospheric state, in that case $T_a = 227$ K and $RHi_a = 90\%$. The purple line denotes the critical mixing line for the Fuel Cell configuration where T_{MAX} and T_{MIN} used for contrail classification are marked (details see text). The light grey lines indicate critical mixing lines for H2 GT and Kerosene GT, respectively.

hPa). If $T_a < T_{\mathrm{MIN}}$ a contrail will always form independent of ambient humidity. (2) T_{MAX} where the critical mixing line touches the liquid saturation curve. If $T_a > T_{\mathrm{MAX}}$ no contrail will form. If $T_{\mathrm{MIN}} < T_a < T_{\mathrm{MAX}}$, a certain minimal ambient water vapor pressure is required to form a contrail, given by: $p_{H_2O\_min} = p_{H_2O\_cm}(T_a)$. Practically, we translate that into a minimum relative humidity in order to directly incorporate the reanalysis RH fields:

$$RHi_{min} = p_{H_2O\_cm}(T_a)/p_{ice}(T_a) \tag{4}$$

Here, $p_{H_2O\_cm}(T_a)$ is the water vapor partial pressure on the critical mixing line at T_a and $p_{ice}(T_a)$ the ice saturation pressure at T_a. If $RHi_a > RHi_{\mathrm{min}}$ a contrail will form and vice versa.

A selection of values for G and the resulting T_{MIN} and T_{MAX} for different pressures (flight altitudes) and the different propulsion systems is given in Table 2. All values decrease with altitude with the H2 FC configuration having the highest threshold temperatures, H2 GT intermediate and Kerosene GT the lowest. It is worth noting, that for H2 FC, T_{MIN} is higher than the freezing threshold temperature of 235 K for all altitudes up to 250 hPa. This means, that for this configuration, the overall temperature threshold is the stricter criterion for contrail formation than the SAC. In the temperature regime $235\ K < T_a < T_{SAC}$ the liquid droplets could either evaporate as soon as the relative humidity in the plume falls below liquid saturation or freeze heterogeneously. Contrails that would form in the latter way are not represented in our approach.

2.3. Reanalysis input data

The CoStat tool is able to operate with global reanalysis data from ERA-5 (Hersbach et al. (2018)) and MERRA-2 (Global Modeling and Assimilation Office, 2015), respectively. Optionally, the tool also allows to import regional subsets of the datasets. Both datasets differ in horizontal and temporal resolution. ERA-5 data are provided on a 0.25° × 0.25° horizontal grid corresponding to a grid cell size of approximately 28 km at the equator. Pressure levels that are relevant for en-route air traffic in ERA-5 are available in 50 hPa steps from 750 to 250 hPa and in 25 hPa steps from 225 hPa to 100 hPa. The native temporal resolution of the ERA dataset is 1h, however it is coarsened to 3h in this study in order to reduce computation time. ERA-5 reanalysis data are implemented in CoStat in netcdf format as obtained by the Copernicus Climate Change Service (Hersbach et al., 2018). The MERRA-2 data used (M2I3NPASM, Global Modeling and Assimilation Office, 2015) are available on a 0.5° longitude and 0.625° latitude grid and a vertical resolution of 50 hPa between 700 hPa and 100 hPa (Bosilovich et al., 2016). The temporal resolution of the MERRA data is 3h. With the temporal resolution of 3h one obtains 8 data points per grid cell per day. For a default analyzed period of one month (30 days) and the default statistical range over 12 years, that implies that the statistics for each pixel in the following map charts comprise 2880 data points. A comparison of potential contrail cirrus cover from both reanalysis data sets is presented in Appendix B.

3. Results

The Potential Contrail Cover and Potential Contrail Cirrus cover from ERA-5 data at 300 hPa for a typical set of parameters is illustrated in Fig. 3. The selected time period is the month of April using 12 years of reanalysis data from years 2010–2021. The default parameters for the different propulsion systems are best estimates for a hypothetical near-future aircraft configuration and are summarized in Table 1. The pressure level of 300 hPa or FL300 is chosen to be representative for regional (~500–1000 nm) cruise altitudes where implementation of H_2 based propulsion system are expected to be realized first. The distribution of Potential Contrail Cover for fuel cell and H2 GT looks almost identical for this configuration. The frequency of contrail formation conditions at mid and high latitudes is close to one with a sharp gradient towards the tropics where the contrail formation frequency drops to almost zero. For Kerosene GT, the tropical band with no contrail formation extends more into the subtropics and contrail formation frequencies stay below 1 even for higher latitudes (consistent with Sausen R. et al. (1998)). Folding the Potential Contrail Cover with the RHi threshold condition ($RHi > 95\%$), one obtains the Potential Contrail Cirrus Cover in the right column of Fig. 3. As to be expected, both maps for fuel cell and H2 GT look identical with distinct high RH spots in the northern hemispheric mid to high latitudes (Pacific, north-western US and Canada, North Atlantic and the northern Asian continent). The southern hemisphere is zonally more homogeneous in comparison but also showing some modulation in the southern mid-latitudes. For Kerosene GT, the patches with enhanced potential contrail cirrus cover are less pronounced, especially over the northern Pacific and the southern part to the north Atlantic ocean where temperatures are too high for contrail formation. This already provides a hint, that the biggest differences between the different propulsion types are expected in regions which are close to threshold conditions concerning contrail formation. For the 300 hPa level, that region is located at the transition from the tropical "no contrail" band to mid latitudes with contrail formation.

3.1. Seasonal variation

The seasonal variation of potential contrail and contrail cirrus is shown in Fig. 4 for Fuel Cell at 300 hPa and four different months (Jan, Apr, Jul, Oct). An animation of the monthly resolved seasonal variation at different altitudes and for the different propulsion types is available as supplementary material online. The band of no contrail formation at low latitudes (both north and south) shifts with the seasonal temperature maximum. In January, contrails from the fuel cell configuration can form at latitudes above 30°N on the northern hemisphere. This transition regions shifts to around 50°N in July. Additionally, the transition towards contrail forming conditions is less sharp in July with values below one extending towards the north pole. In the southern hemisphere we observe the corresponding pattern with the least sharp transition in January and less zonal modulation. The general seasonal characteristic is similar for altitudes below 300 hPa with the low latitudes band of no contrails extending further towards high latitudes with decreasing altitude. In July, contrail formation for the fuel cell setting is only possible in the polar regions at 350 hPa and below. At 250 hPa the low latitude band closes and contrails are likely to form also in the tropics, the only exception being the Asian summer monsoon region where a bubble with no contrail forming conditions appears in June over India and extends towards the middle east in the summer months. Compared to the potential contrail cover spanning a range from zero to one, the potential contrail cirrus cover (right column in Fig. 4) has significantly lower

Table 2
SAC parameters for the different propulsion types.

	Fuel Cell (U = 0.7V)			H2 GT (η = 0.35)			Kerosene GT (η = 0.35)		
Pressure [hPa]	G [Pa/K]	TMIN [K]	TMAX [K]	G [Pa/K]	TMIN [K]	TMAX [K]	G [Pa/K]	TMIN [K]	TMAX [K]
250	7.13	236.82	247.89	4.62	232.14	242.70	1.82	222.81	232.31
300	8.55	238.85	250.15	5.55	234.08	244.85	2.19	224.57	234.27
350	9.98	240.61	252.10	6.47	235.75	246.71	2.55	226.08	235.96
400	11.40	242.16	253.83	7.39	237.23	248.34	2.92	227.41	237.44

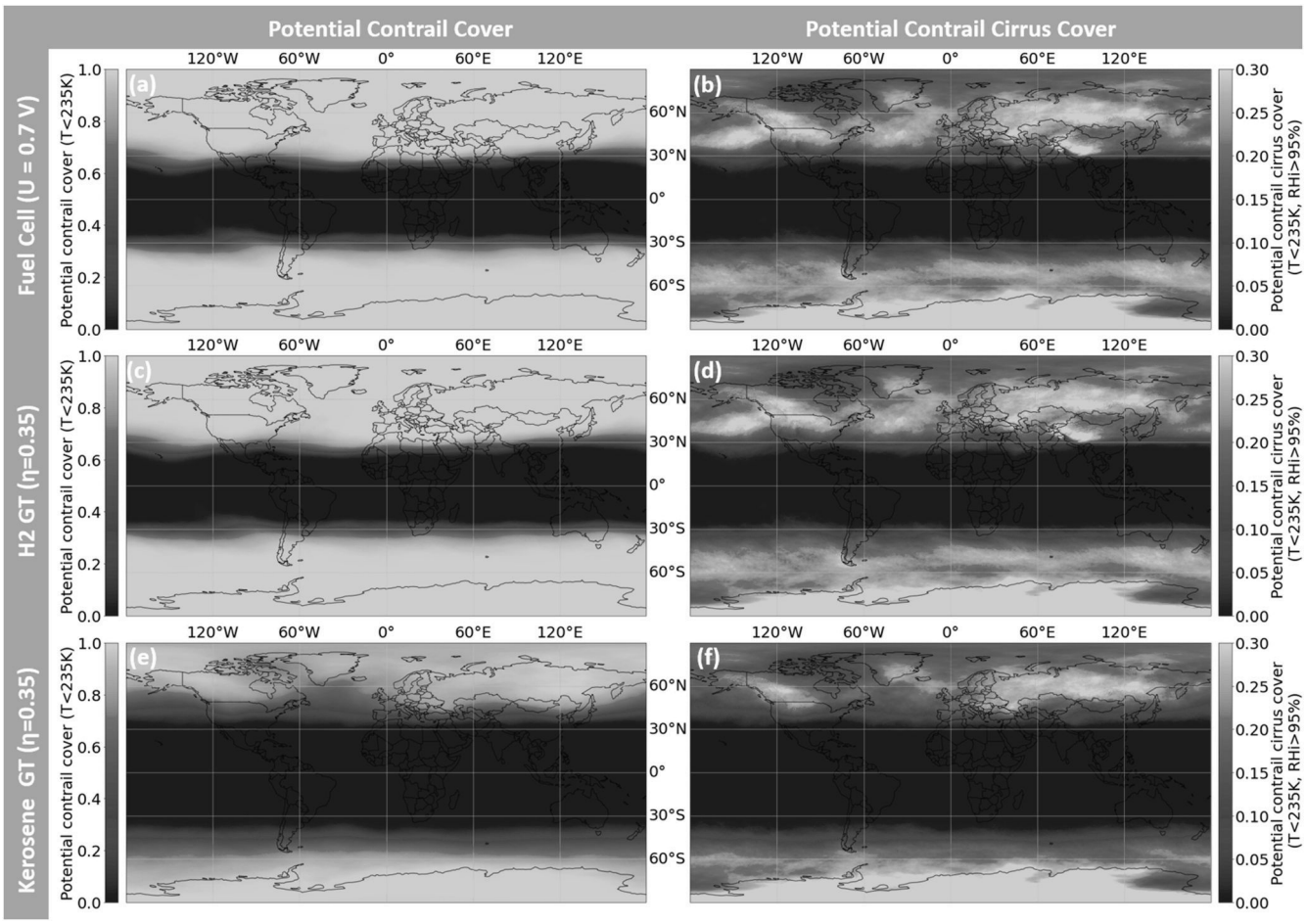

Fig. 3. Potential Contrail Cover (left) and Potential Contrail Cirrus Cover (right) using global ERA-5 reanalysis data with 3 h time resolution. The statistic is performed for April for years 2010–2021 at a pressure level of 300 hPa. Potential Contrail Cover is calculated using the threshold temperatures as from Table 2 and an absolute temperature threshold of 235 K. For Potential Contrail Cirrus Cover, an additional filter for $RHi > 95\%$ is applied. (a) is Potential Contrail Cover and (b) Potential Contrail Cirrus Cover for a fuel cell propulsion at an operating voltage of $U = 0.7\ V$, (c) and (d) for a hydrogen powered gas turbine with an overall propulsion efficiency of $\eta = 0.35$, (e) and (f) for a regular kerosene combustion engine with an overall propulsion efficiency of $\eta = 0.35$. Difference plots of hydrogen vs. kerosene propulsion are shown in Fig. 5.

numbers (between zero and 0.3). It follows the same meridional pattern as the contrail cover, but with much lower values for the contrail cirrus frequency and some distinct high humidity hot-spots. On of these hot-spots is located over the northeast Pacific and the western North American continent and can be observed throughout the year following the general northward shift in boreal summer. The other two distinct regions with statistically enhanced humidity are over the North Atlantic and Greenland and over the central Eurasian continent. On the southern hemisphere, we find higher frequencies for potential contrail cirrus cover only over the Antarctic landmass. The location of regions with enhanced humidity is very similar for the levels above (200 hPa, 225 hPa, 250 hPa) and below (350 hPa and 400 hPa) the 300 hPa level shown.

3.2. Global difference between propulsion types

In order to assess the differences between propulsion types, the difference of potential contrail and contrail cirrus cover between Fuel Cell and Kerosene GT configuration at four different altitude levels for April is plotted in Fig. 5. Since contrail formation of H2 FC and H2 GT behaves almost identical, this can be generalized as difference between H_2 based and kerosene propulsion. Due to the higher water vapor emissions, the Fuel Cell always produces more contrails than the Kerosene GT. However, we observe significant altitude dependent characteristics of the difference. At 250 hPa, the highest difference in contrail formation is found in the tropical band (Fig. 5 (a)) where temperatures are always below threshold for Fuel Cell while above threshold for Kerosene GT. At this altitude, H_2 propulsion always produces contrails all over the globe. The high difference in potential contrail cover at this altitude directly transfers to the potential contrail cirrus cover (Fig. 5 (b)) with most pronounced features in the continental and Asian ITCZ and the south Pacific ocean. These general characteristics are not only found for April but also for the other seasons with the tropical band shifting with the ITCZ over the year. At lower altitudes (300 hPa down to 400 hPa, Fig. 5 (c–e,g)), the tropical band with no contrail formation exists for both propulsion types resulting in no difference there. As already indicated above, the biggest difference at 300 hPa is observed at the edges of the tropical band around 30 to 40°N (and south). At higher latitudes, the difference reduces significantly, implying that temperatures are far lower than threshold to allow contrail formation independent of the propulsion type. As the meridional extension of the tropical band increases with decreasing altitude, the zonal band with highest differences moves to higher latitudes for 350 hPa and 400 hPa. Interestingly, the bands do not only shift in latitude but also the magnitude of the difference decreases with decreasing altitude since contrail formation frequencies start to decrease for the fuel cell configuration at low altitudes. The seasonal cycle at lower altitudes follows the same pattern as for the high altitudes with a northward shift of all features in boreal summer

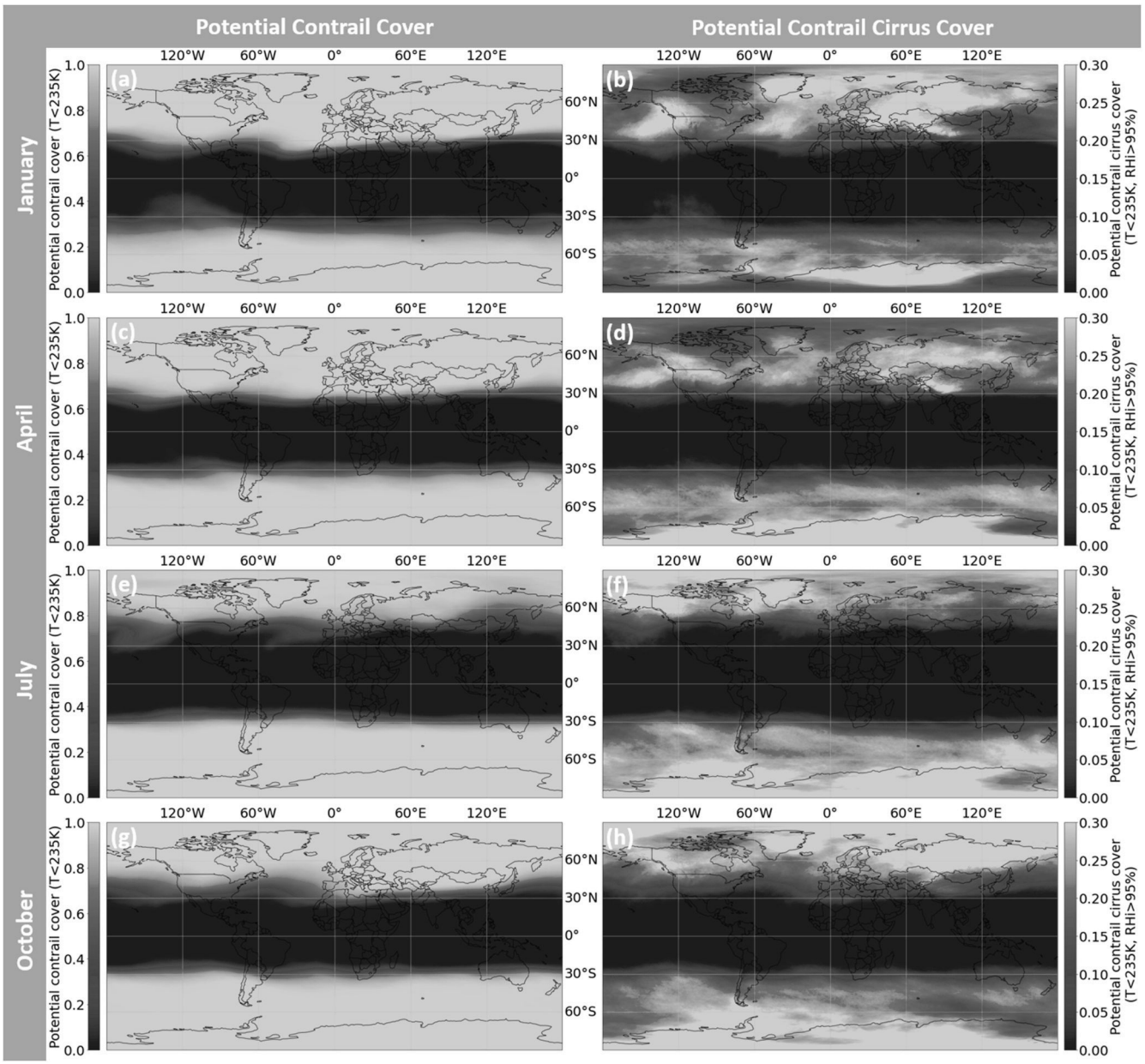

Fig. 4. Seasonal variation of Potential Contrail cover (left) and Potential Contrail Cirrus Cover (right) for Fuel Cell at 300 hPa. The rows are snapshots of Jan, Apr, Jul, and Oct representing the four different seasons. The contrail formation bands at high latitudes shift north in summer leading to less Potential Contrail Cirrus Cover in mid-latitudes.

and a southward shift in winter. Comparing the H2 FC to the H2 GT setting, there is less difference as can be expected from the higher G-factors for H2 GT compared to Kerosene GT. In fact, significant differences are only observed at 250 hPa while there are no differences at the lower altitudes. This can be explained directly by the SAC threshold temperature T_{min} (see Table 2) and the set absolute threshold temperature for contrail ice formation $T_{thres} < 235$ K. At altitudes below 250 hPa, T_{min} is greater than 235 K for both H_2 propulsion variants. That means, that contrail formation will always happen for both as soon as ambient temperature falls below $T_{thres} = 235$ K. Even for H2 GT at 250 hPa it needs to be very dry and close to threshold conditions that no contrail forms. Thus, no big difference between the two H_2 settings is expected in the investigated altitude range.

3.3. Consequences for regions with high regional air traffic

Since the most likely scenario for a mid-term replacement of kerosene powered aircraft by H_2 based propulsion systems is on regional and short haul flights, we selected the three regions with highest air traffic density in a similar approach as in Teoh et al. (2024)) to investigate the potential changes in contrails and contrail cirrus from a hypothetical H2 powered fleet. Following the latest ICAO air traffic report from 2021, around 92% of all domestic passenger flight kilometers are attributed to northern America, Europe or Southeast Asia, respectively (ICAO, 2021). These three regions are selected as shown in Fig. 6 and named intuitively as USA (including small parts of Canada and Mexico and excluding Alaska and Hawaii), Central Europe (extending to Southern and Western Europe) and Southeast Asia in order to compare seasonal variation and altitude dependence of potential contrail (cirrus) cover for the different propulsion settings. The three graphs at the bottom in Fig. 6 show the

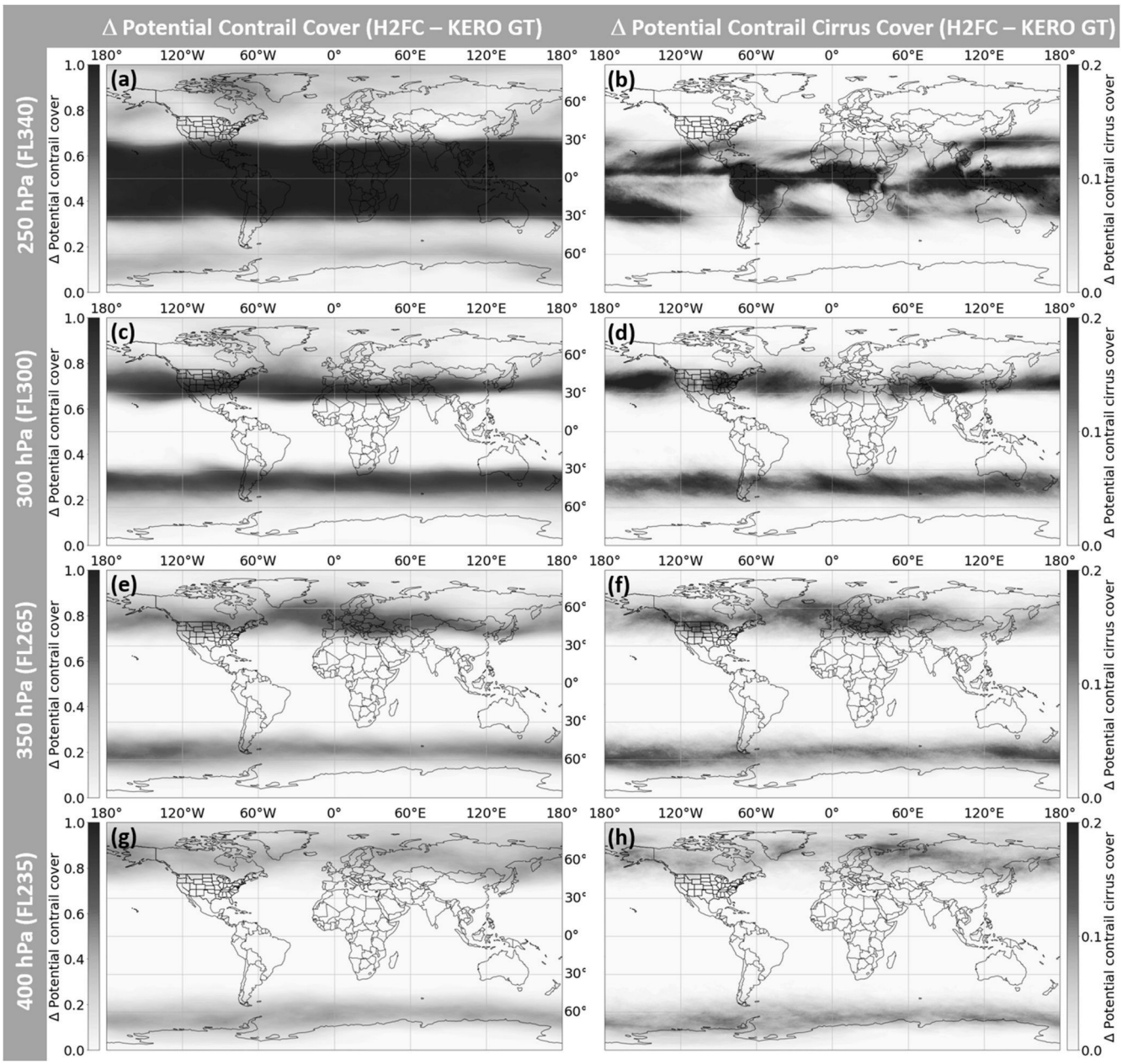

Fig. 5. Difference in Potential Contrail Cover (left) and Potential Contrail Cirrus Cover (right) between Fuel Cell ($U = 0.7\ V$) and Kerosene GT ($\eta = 0.35$) propulsion for April at four different altitudes based on 3-hourly global ERA-5 data from 2010 to 2021.

seasonal variation for the H2 FC setting at 300 hPa for each region with potential contrail cover as dashed lines and potential contrail cirrus cover as solid lines. The filled areas and dotted lines are the 25–75 percentile range and the 5–95 percentile range respectively. The percentile ranges represent the spatial variability of both quantities within the selected regions. The potential contrail cover (dashed lines in Fig. 6) exhibit a similar seasonal characteristic with low values in summer compared to winter while absolute values strongly increase with latitude. Values are highest in Europe (with 100% throughout the whole winter season), followed by USA and Southeast Asia, where highest values in February merely reach 40%. Also the spatial variability (represented by the IQR (interquartile range) differs substantially with highest values in European summer, Southeast Asian winter and almost constant medium values in the US throughout the year. High peak values in IQR are caused by the transition of the low latitude "no contrail" band through the respective regions. The potential contrail cirrus cover (solid lines in Fig. 6) shows a similar behaviour but with less absolute variation. For Europe and US, values are capped at around 20% reflecting the typical frequency of RHi > 95% (compare RHi distributions in Appendix B). Folded with the frequency of contrail formation, the potential contrail cirrus cover for all investigated levels drops to almost zero in the US in summer, while staying at around 10% in Europe. Those values are significantly smaller in the Southeast Asian box where peak values in February and March reach only up to around 8% while being close to zero for almost half a year in summer.

3.4. Regional and seasonal variation of potential contrail cirrus cover

In order to obtain a comprehensive picture of seasonal, regional, altitude and propulsion type dependence of potential contrail cirrus occurrence, Fig. 7 shows mean values of potential contrail cover (dashed) and potential contrail cirrus cover (solid) for four different altitudes (rows), the three regions (columns) from higher to lower latitudes and the three different propulsion types (distinguished by colors).

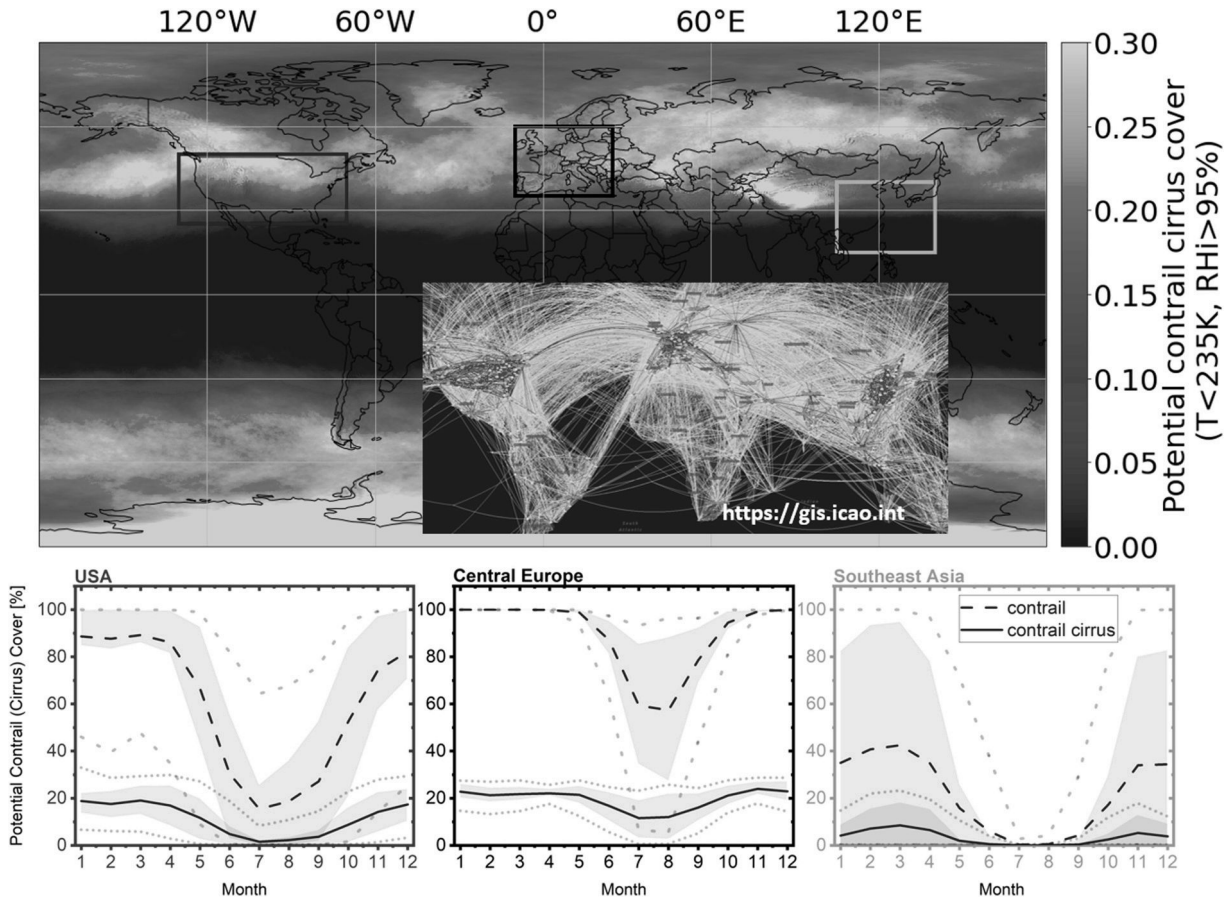

Fig. 6. Hot-spot regions for regional air traffic, selected according to the air traffic density from ICAO for 2018 (ICAO, 2018). The world map shows potential contrail cirrus cover in March at 300 hPa. USA, Central Europe and Southeast Asia were identified as region with most dense regional air traffic, further statistical analyzes are performed for all values within the respective boxes. The lower three panels show mean values of Potential Contrail cover (dashed lines) and Potential Contrail Cirrus Cover (solid lines) for Fuel Cell propulsion at 300 hPa in dependence of the season. Shaded areas and dotted lines mark the IQR and the 5th an 95th percentile of the spatial distribution within the box, respectively.

Adjacent pressure levels are shown in Appendix C. As already qualitatively described above, the potential contrail cover decreases from higher to lower altitudes and also from higher to lower mean latitudes (from Central Europe to Southeast Asia). Thereby, it extends over the whole span of almost 100% at 225 hPa (FL360) to very low values in Southeast Asia at 350 hPa (FL265). Since all investigated regions are on the northern hemisphere, the seasonal cycle is in phase with lowest values in summer and highest values in winter. As expected from the lower threshold temperatures (Table 2), values for potential contrail cover for Kerosene GT are lower compared to H_2 propulsion. Results from H2 FC and H2 GT are very similar and differ only at altitudes of 250 hPa, where T_{MIN} falls below 235 K. At lower altitudes, contrail formation is limited by the freezing threshold and not by SAC for both H_2 propulsion settings.

The observed features in contrail formation do not transfer directly to the potential contrail cirrus cover which has a higher climate relevance, underlining the interaction between temperature and humidity fields. Looking e.g. at Central Europe at 225 hPa or 250 hPa, there is almost no difference in potential contrail cirrus cover for all propulsion types despite a large difference in potential contrail formation between H_2 and kerosene propulsion. This implies, that the condition of being humid enough for persistent contrails and at the same time being too warm for contrail formation does only rarely occur in the atmosphere. It furthermore implies, that for these specific propulsion settings and region, there is not much difference in climate relevant persistent contrails from Kerosene or H_2 propulsion. The situation looks different for regions with lower mean latitudes at 225 hPa and 250 hPa, where contrail formation from Kerosene GT drops lower during the summer also reducing potential contrail cirrus cover. This leads to up to 18 percentage points higher values in potential contrail cirrus in summer and a still negligible difference in winter. For Southeast Asia, there is even a slight anti-correlation between potential contrail and contrail cirrus cover, again stressing the need to always look at both temperature and humidity. The seasonal dependence in USA at 225 hPa and 250 hPa can be qualitatively found again in Central Europe but always one altitude step below. The seasonal structure of the difference between H_2 and Kerosene propulsion changes when looking at lower altitudes 350 hPa in Central Europe, 350 and 300 hPa in USA), where we observe maximum differences in winter while differences and absolute values approach zero in summer. Comparing Central Europe and the US region in Fig. 7, a variation of mean latitude or altitude seems to trigger similar changes in potential contrail cirrus cover. Thus, the issue of climate effective contrail cirrus is more relevant for the European than for the Asian region with USA sitting in an intermediate position. Furthermore, we observe a strong interplay between temperature and humidity: while there is almost no change in potential contrail cirrus when contrail formation frequencies vary between 100 and roughly 50% there is a significant reduction in contrail cirrus when contrail formation frequencies fall below 50%, implying that atmospheric conditions are most sensitive in the above described transition regions. On the other hand, once a certain threshold in contrail formation frequency is reached, the actual propulsion type is of minor importance for potential contrail cirrus.

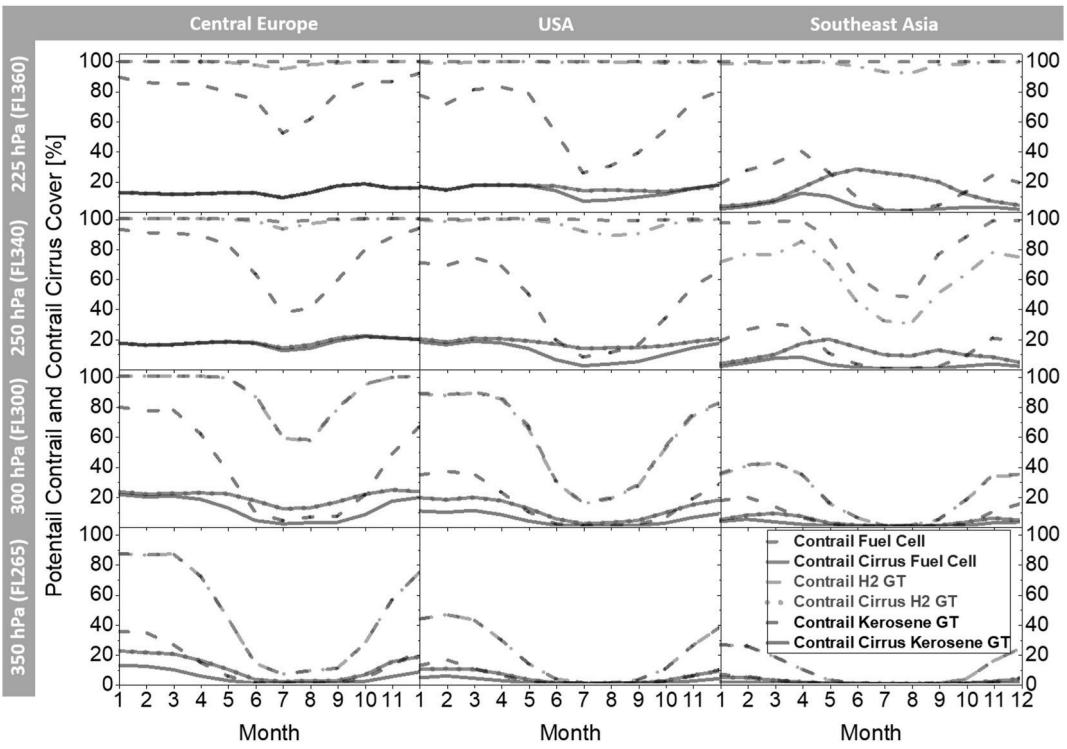

Fig. 7. Seasonal variation of mean values for Potential Contrail Cover (dashed lines) and Potential Contrail Cirrus Cover (solid lines) from Fuel Cell (blue), H2 GT (red) and Kerosene GT (black) for pressure levels 225 hPa, 250 hPa, 300 hPa and 350 hPa (rows) and the three different hot-spot regions (columns).

4. Discussion and outlook

Since contrail formation threshold temperatures are very sensitive to latitude, altitude and season, it is difficult to provide one simple answer on contrail cirrus cover would be affected when changing aircraft propulsion systems from kerosene to H_2 based propulsion. In our analysis, we find parameter combinations where there is hardly any difference between kerosene and H_2 propulsion with respect to the potential for contrail cirrus, like e.g. the winter months at 250 hPa throughout all three investigated regions. There, the ambient temperature is typically far below threshold conditions for all combustion types and contrail cirrus formation is only limited by the occurrence of supersaturated regions. As a rough guide to the eye, propulsion independent contrail cirrus frequency is typically observed in a regime when potential contrail frequency for kerosene combustion exceeds 50%. For a range of atmospheric conditions where the frequency of contrail formation is between 0 and 50% for kerosene GT and 50 and 100% for H2 GT and H2 FC, we observe a significant difference in potential contrail cirrus frequencies between the propulsion types. In this "close to threshold" regime, the additional water vapor from H_2 propulsion folded with the supersaturation condition can lead to differences of up to 15% absolute in contrail cirrus frequency. This feature shifts from winter to summer with increasing altitude and decreasing mean latitude. Similar seasonal dependencies can e.g. be observed in Europe at 350 hPa (300 hPa) and USA at 300 hPa (250 hPa). In the third "above threshold" regime where potential contrail frequencies drop below around 50% also for H_2 propulsion, the difference in potential contrail cirrus decreases again due to the overall drop in occurrence frequencies. As conclusion, we only observe significant differences in potential contrail cirrus frequency for different propulsion types in a "close to threshold regime" where frequencies of contrail formation are below (above) a certain limit for kerosene (H_2 propulsion). That limit seems to lie somewhere around 50%. When mean atmospheric conditions are either far below or far above threshold conditions, the additional water vapor in the H_2 propulsion exhaust does not alter contrail cirrus frequencies significantly. The regions where the contrail cirrus penalty for H_2 powered aircraft is negligible can provide a strong lever when optimizing their impact on the atmospheric radiation budget.

As this study focuses on a statistical evaluation of the ambient atmospheric conditions relevant for contrail and contrail cirrus formation from different propulsion types, detailed properties and evolution of single contrails as e.g. tracked in CoCip (Schumann (2012); Teoh et al. (2022a)) are not covered. Also, an increase in potential contrail cirrus cover does not necessarily lead to an increased climate impact as e.g. shown in (Teoh et al., 2022b). The climate impact of contrail cirrus strongly depends on the individual meteorological situation, on ice particle size and number concentration controlling the optical thickness which are controlled by available particle nuclei, on contrail lifetime controlled by ambient humidity as well as on the diurnal solar cycle (Teoh et al., 2022a). In order to evaluate the potential additional climate impact of contrails produced from H_2 propulsion, it is thus essential to know how exactly the surplus water compared to kerosene combustion is emitted. Here we assume a hot gaseous emission similar to kerosene jet engines. However, an emission of a much colder spray of small liquid droplets due to recuperation of exhaust heat and subsequent condensation within the aircraft is also a possible scenario for a fuel cell powered aircraft (Adler and Martins, 2023). On the one hand, this could lead to even more frequent contrail formation due to lower exhaust gas temperature. On the other hand, initially bigger droplets may lead to reduced optical thickness and a significantly reduced lifetime due to faster sedimentation Bier et al. (2024).

After a contrail has formed, the most critical parameter for climate relevant contrail cirrus is obviously the relative humidity with respect to ice along the contrails lifetime. In this study, we chose to work with the original RH fields from the reanalysis in combination with a threshold of 95%. Li et al. (2023) found contrail cirrus with lifetimes of several hours in slightly subsaturated conditions in airborne measurements, indicating that a below saturation threshold is a realistic assumption when assessing climate relevant contrail cirrus. Alternative approaches applied correction methods to the RH fields using correction factors

(Schumann et al., 2015), parameterized correction as in Teoh et al. (2022a) or statistical methods as in Wolf et al. (2023); Hofer et al. (2024b). Since we only classify data in above and below threshold in this study and do not process e.g. the RH distribution in supersaturated conditions, all three approaches yield almost identical results when run through the CoStat algorithm. However, the analysis is prone to uncertainties or biases in the model temperature and RH fields, e.g. the wet bias of ECMWF at the tropopause (Kaufmann et al., 2018; Dyroff et al., 2015; Gierens et al., 2020; Hofer et al., 2024b; Agarwal et al., 2022).

Compared to contrail studies on pure kerosene combustion, not only the RH threshold but also the temperature threshold at 235 K plays an important role. For typical kerosene conditions, T_{MAX} for contrail formation is below 235 K down to pressure levels of around 350 hPa (see Table 2), implying that contrails only form in the pure ice regime. This is different for the H_2 propulsion settings where e.g. even T_{MIN} is above 235 K up to 250 hPa for the Fuel Cell setup. This implies, that the set temperature threshold is actually the stricter condition than the SAC and contrails can potentially form in a mixed phase temperature regime. Since we can only speculate about the characteristics of such mixed phase contrails, they are explicitly not covered in the herein applied CoStat algorithm. Together with further possible differences in especially the Fuel Cell propulsion, like spontaneous nucleation of particles due to very high local supersaturation or particle formation within the engine altering the classical SAC approach, this might become a topic for further investigations.

CRediT authorship contribution statement

Stefan Kaufmann: Writing – original draft, Visualization, Software, Methodology, Investigation, Formal analysis, Conceptualization. **Rebecca Dischl:** Writing – review & editing, Software. **Christiane Voigt:** Writing – review & editing, Validation, Supervision, Resources, Funding acquisition.

Declaration of competing interest

The authors declare that they have no known competing financial interests or personal relationships that could have appeared to influence the work reported in this paper.

Data availability

Data will be made available on request.

Acknowledgements

This work acknowledges funding by the Aviation Research Programme of the German Federal Government (LuFo VI-2) within Project no. 20M2110B (DINA2030+), by DFG within projects no. 510826369 (ECOCON) and no. 522359172 (SPP HALO) and by the European Union's Horizon Europe and SESAR programs under grant no. 101114785 (CONCERTO) and grant no. 101114613 (CICONIA). ERA-5 data are provided by the European Copernicus Data Service. MERRA-2 data were provided by the NASA Global Modelling and Assimilation Office. The authors would like to thank Runa Ostermeier and Klara Bosch for their improvements to the CoStat algorithm. The authors would also like to thank Klaus Gierens for valuable discussions of the results and comments on the manuscript.

Appendix A. Interannual and diurnal variability

In order to more thoroughly cover the variability of potential contrail and contrail cirrus cover, temporal variability has to be considered in addition to the spatial variability which is depicted in Fig. 6. The maximum interannual variability found in potential contrail cover is typically around + - 15%. The variability decreases when potential contrail cover approaches either 0 or 100% (Fig A.8). The interannual variability for potential contrail cirrus cover is lower due to lower absolute numbers at around + -6 percentage points. The high interannual variability indicates, that the frequency of weather systems with high humidity and cold temperatures is not constant for the investigated mid-latitude regions and investigated time steps of one month. This is consistent with global modelling studies by Frömming et al. (2021) who found that the climate impact of aircraft emissions is crucially dependent on its location relative to synoptic weather systems in the North Atlantic. In contrast, the diurnal variability can be neglected compared to spatial and interannual variability. There, maximum differences in potential contrail and contrail cirrus cover between day (9-16UT) and night (21-4UT) are consistently below 0.5% also indicating that larger scale synoptic weather systems are the main driver for regions susceptible to contrail (cirrus) formation. However, when looking at the contrail climate impact and not only at contrail cover, the daytime is a crucial parameter since nighttime contrails are always warming while daytime contrail might be either warming or cooling (e.g. Teoh et al. (2022a)).

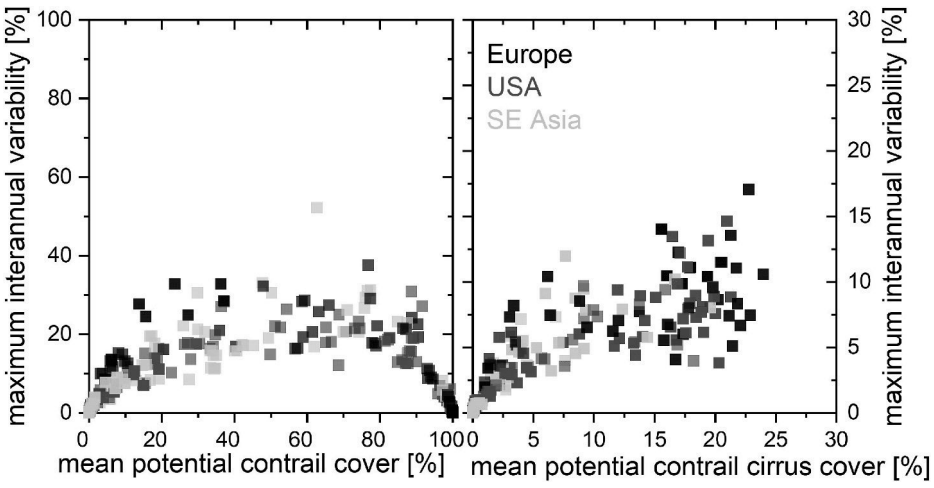

Fig. A.8. Interannual variability of mean potential contrail cover (left) and potential contrail cirrus cover (right) in the three hot-spot regions. The maximum variability is the difference between the year with maximum and minimum values.

Appendix B. Comparison of ERA and MERRA reanalysis data sets

Dischl et al. (2022) have shown that the choice of the reanalysis data set has a significant influence on the results on potential contrail cover when comparing ERA-5 and the much coarser NCEP input data. In order to compare reanalysis data with comparable resolution and implementation of physical processes, we here use MERRA-2 data to compare to ERA-5. MERRA and ERA data are processed identically within the CoStat tool, the only difference being the different spatial resolution of the temperature and relative humidity input fields. For the following comparison, we reduced both global data sets to the finest common grid, which is 0.5° in latitude, 1.25° in longitude. As described above, we also use a reduced temporal resolution of the ERA data from its 1-hourly native resolution to 3-hourly data matching the temporal resolution of MERRA. Generally both reanalysis data sets produce very similar spatial and seasonal patterns in potential contrail (cirrus) cover. However, we observe also systematic differences between both models with different characteristics at different altitudes.The MERRA-2 data used (M2I3NPASM, Global Modeling and Assimilation Office, 2015) are available on a 0.5° longitude and 0.625° latitude grid and a vertical resolution of 50 hPa between 700 hPa and 100 hPa (Bosilovich et al., 2016). The temporal resolution of the MERRA data is 3h.

Figure B.9 shows the difference in potential contrail cover (left column) and potential contrail cirrus cover (right column) for the Fuel Cell configuration for April at three different altitudes (400 hPa, 300 hPa, 250 hPa) when using ERA or MERRA as data input (difference is calculated as MERRA-ERA). Differences are given as absolute numbers of the respective frequencies. In the following, the reasons for differences in potential contrail (cirrus) cover are analyzed using zonal means of temperature differences (Fig. B.10 left column), RH differences (Fig. B.10 middle column) and the fraction of RH values above 95% from both models (Fig. B.10 right column) (in combination with zonal histograms of RH from both models (Fig. B.11)). For the ΔT and ΔRH column in figure B.10, differences are calculated for each point in space and time for the years 2010–2021. Afterwards, the differences are zonally averaged in 30° bins to obtain the six values per altitude as shown in the figure. Both quantities exhibit a systematic difference. Temperature means in MERRA are constantly higher (except the Antarctic latitudes at 250 hPa) with highest differences in the tropics which are decreasing towards higher latitudes. Similar, MERRA shows also higher RH mean values than ERA with no clear latitude dependency at 250 hPa and a again more pronounced tropical bias at lower altitudes. At mid and high latitudes at 400 hPa, the difference even shifts towards a small dry bias in MERRA compared to ERA. However, looking at the fraction of RH values being greater than 95% which is the relevant measure for the potential contrail cirrus cover reveals a different latitudinal behavior (right column in Fig. B.10). Using that measure, ERA consistently shows higher values at high and mid latitudes (leading to more contrail cirrus in ERA) while having lower values in the tropics. This is consistent with the general patterns in potential contrail cirrus cover in Fig. B.9 (right column). The seeming discrepancy between ΔRH and the potential contrail cirrus cover (fraction of $RHi > 95\%$) also indicates, that the RH representation in both models differs for dry and close-to-saturation conditions, respectively, which is confirmed by the RHi distributions for each data set (Fig. B.11). Looking specifically at the differences in potential contrail (cirrus) cover, at 250 hPa, potential contrail cover (Fig. B.9 a) is higher for ERA in the tropics indicated by the blue tropical belt. The reason are the described lower temperatures in the tropics for ERA (Fig. B.10). At this altitude, the temperature difference is only relevant in the tropics since the atmosphere is far below threshold conditions at higher latitudes. At higher latitudes, the potential contrail cover equals one for both data sets (a contrail is always produced), so there is no difference there. In contrast to the potential contrail cover, the potential contrail cirrus cover in the tropics is higher in MERRA, which is consistent with the higher fraction of RH values above 95%. At higher latitudes, the difference shifts towards ERA seeing more potential contrail cirrus caused by the higher fraction of values above 95% in those regions. It has to be noted, that the general patterns are broken by e.g. spots of higher potential contrail cirrus cover in ERA over Central Africa and the northern part of South America or higher probabilities in MERRA along the US east coast (Fig. B.9 b). At 300 hPa the potential contrail cover differs in the subtropics in the transition from no contrail to contrail conditions (Fig. B.9 c) where ERA again has the tendency to more contrail formation. For potential contrail cirrus in Fig. B.9 d ERA shows higher frequencies for almost all regions expect the North American coasts, the Andes and the Tibetian Plateau. The magnitude of the difference grows with latitude, indicating a different meridional gradient in ice saturation between the models. At 400 hPa there is almost no difference in potential contrail cover between the two models due to the sharp gradient in the subtropics not being present there (Fig. B.9 e). The situation for the potential contrail cirrus cover looks similar to 300 hPa: in regions where contrails form (at 400 hPa in the high latitudes only) ERA has a higher frequency of potential contrail cirrus (Fig. B.9 f). Generally, two characteristic features of the model comparison can be noted. First, significant differences in potential contrail cover are found in regions close to threshold conditions with ERA seeing more contrails due to generally lower temperatures. Second, model differences in potential contrail cirrus cover are substantially different compared to potential contrail cover. Potential contrail cirrus cover is generally higher in ERA at mid and high latitudes and lower in the tropics compared to MERRA caused by a substantially different representation of the RH distribution in both models.

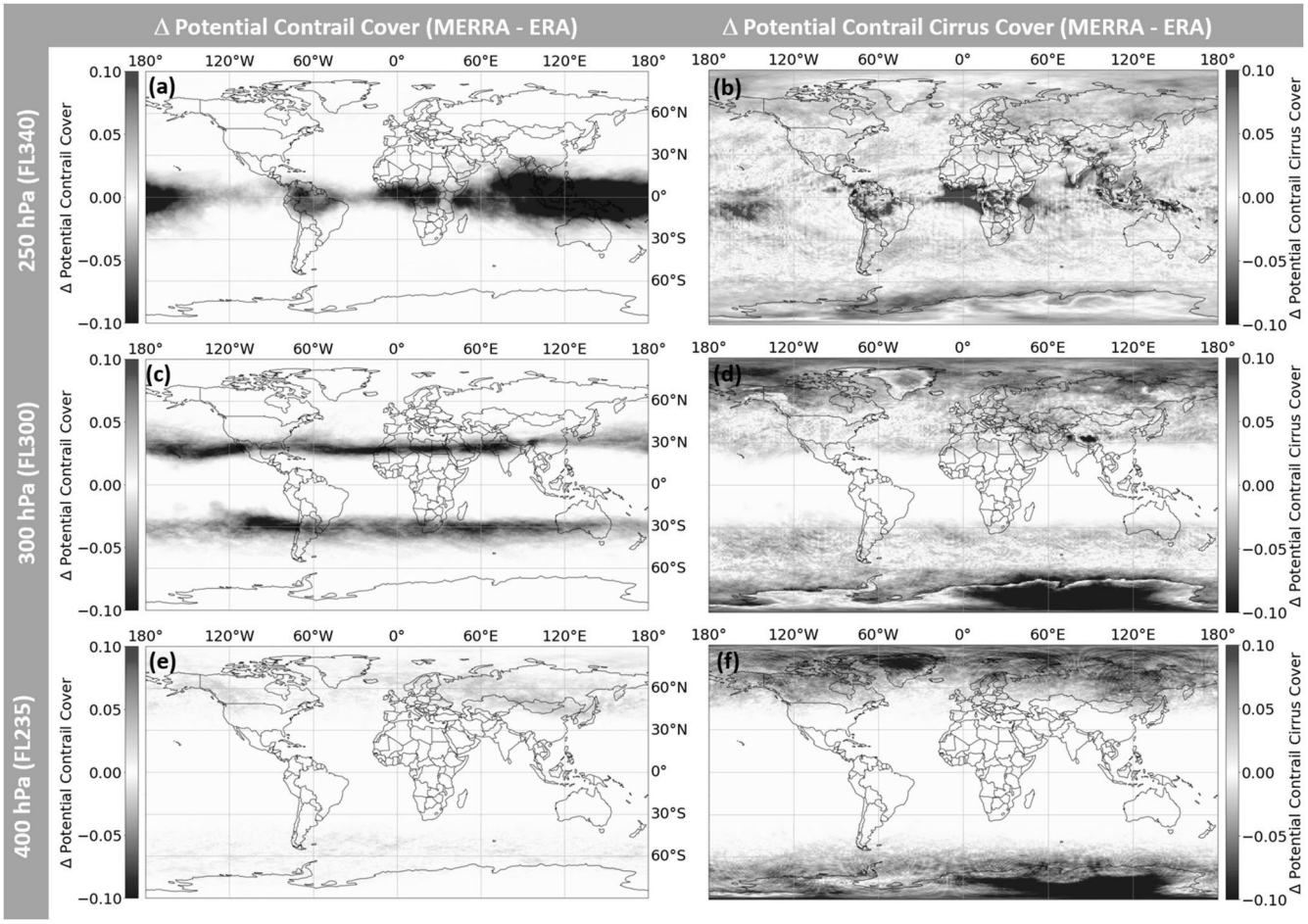

Fig. B.9. Difference of Potential Contrail Cover (left) and Potential Contrail Cirrus Cover (right) between MERRA and ERA for Fuel Cell propulsion at three different levels (250 hPa, 300 hPa and 400 hPa) in April. Blue colors indicate higher values for ERA in Potential Contrail (Cirrus) Cover, red colors indicate higher values in MERRA.

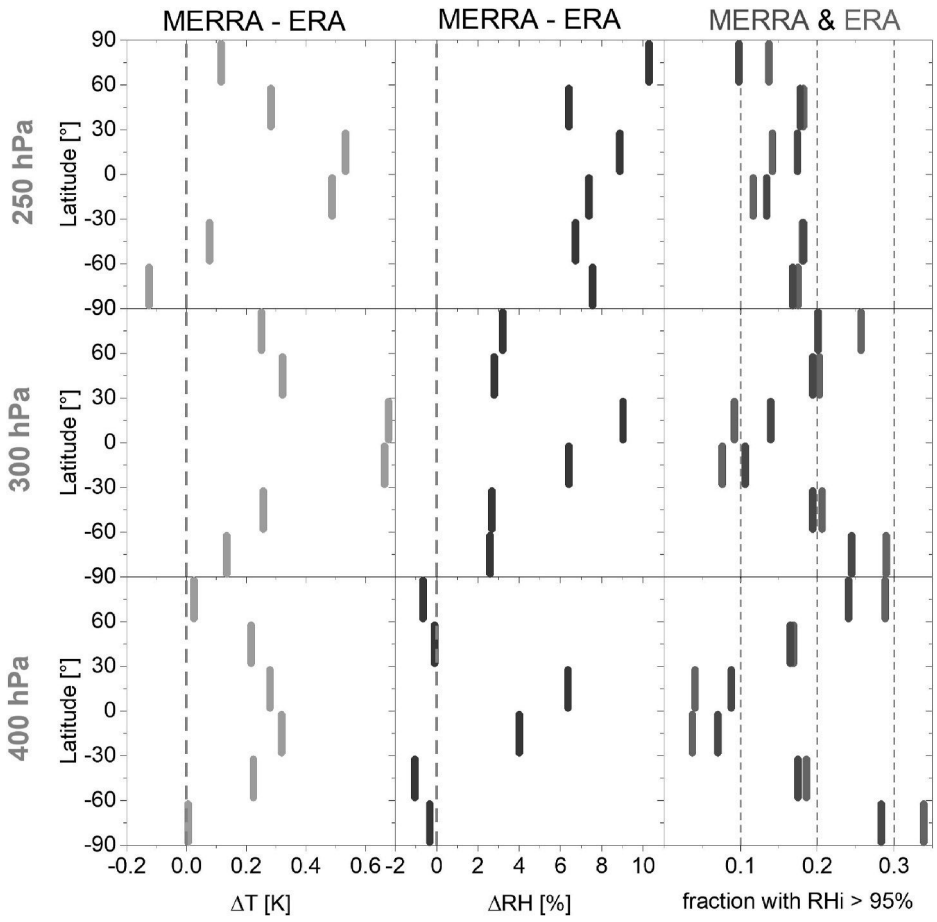

Fig. B.10. Zonal mean values of temperature difference (left column) and RH difference (middle columns) between MERRA and ERA. The right column shows zonal means of the fraction of RH values above 95% for both models.

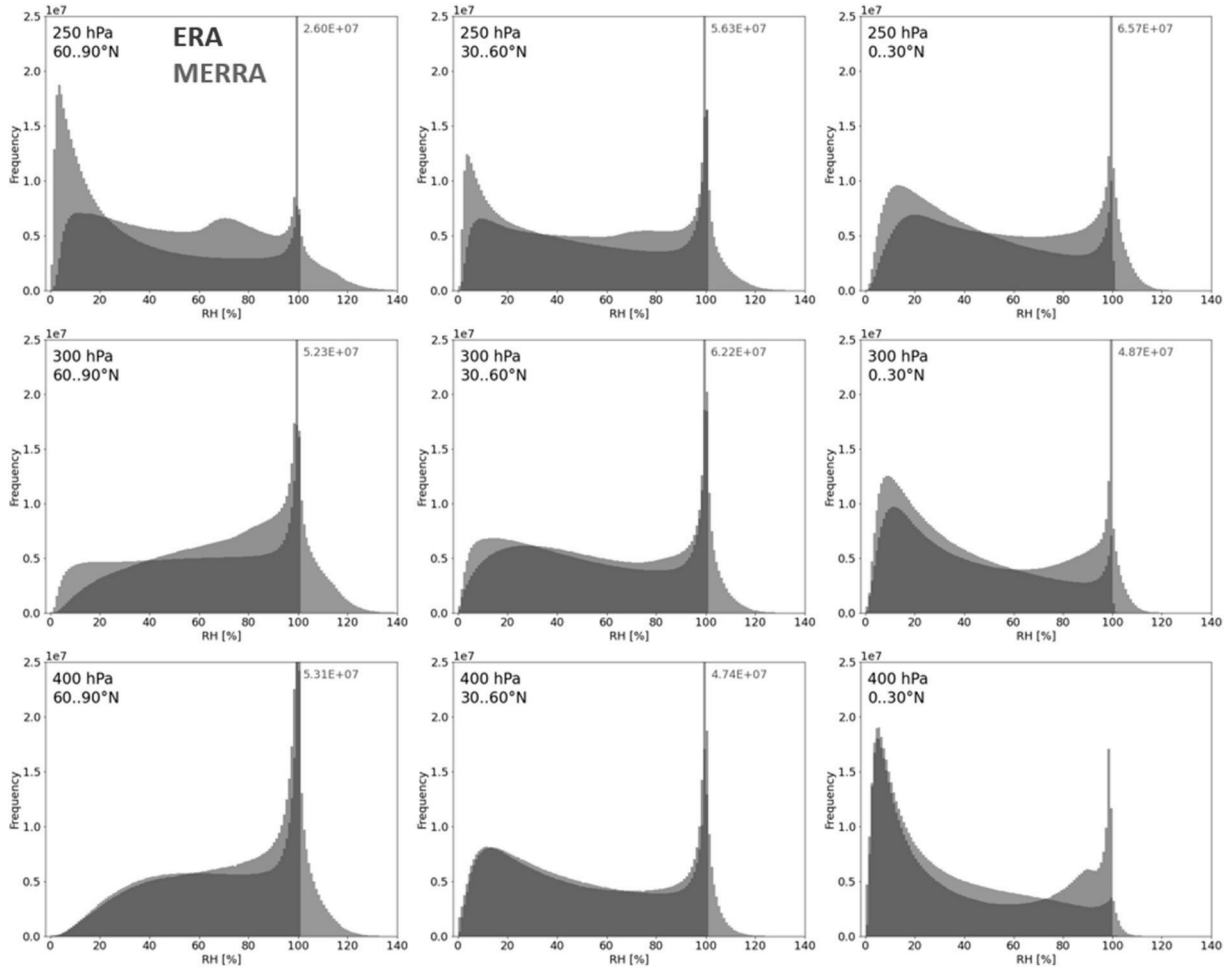

Fig. B.11. Zonal RHi distributions for ERA and MERRA from high latitudes (left) to tropics (right) at three different pressure levels (250, 300 and 400 hPa). While MERRA has no ice supersaturation, the peak at saturation is more pronounced in MERRA data. Therefore, maximum values out of scale are noted in the respective plots.

Appendix C. Potential contrail and contrail cirrus at 200 and 400 hPa

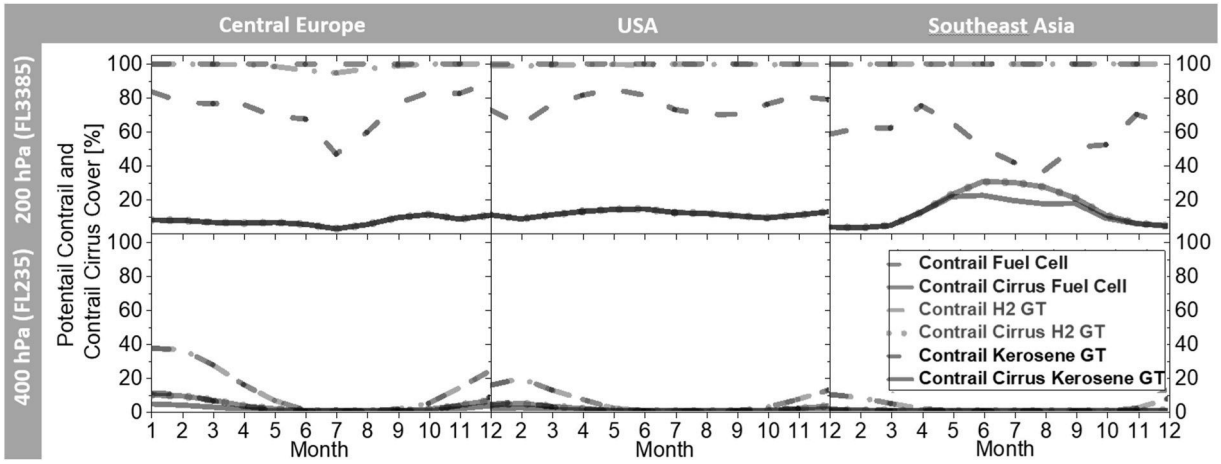

Fig. C.12. Seasonal variation of mean values for Potential Contrail Cover (dashed) and Potential Contrail Cirrus Cover (solid lines and red dotted line) for complementary pressure levels to Fig. 7 at 200 and 400 hPa.

References

Adler, E.J., Martins, J.R., 2023. Hydrogen-powered aircraft: fundamental concepts, key technologies, and environmental impacts. Prog. Aero. Sci. 141, 100922 special Issue on Green Aviation.

Agarwal, A., Meijer, V.R., Eastham, S.D., Speth, R.L., Barrett, S.R.H., 2022. Reanalysis-driven simulations may overestimate persistent contrail formation by 100%–250. Environ. Res. Lett. 17 (1), 014045.

Airbus, 2024. Airbus zeroe programme. https://www.airbus.com/en/innovation/low-carbon-aviation/hydrogen/zeroe. (Accessed 19 April 2024).

Bier, A., Unterstrasser, S., Zink, J., Hillenbrand, D., Jurkat-Witschas, T., Lottermoser, A., 2024. Contrail formation on ambient aerosol particles for aircraft with hydrogen combustion: a box model trajectory study. Atmos. Chem. Phys. 24 (4), 2319–2344.

Bock, L., Burkhardt, U., 2019. Contrail cirrus radiative forcing for future air traffic. Atmos. Chem. Phys. 19 (12), 8163–8174.

Borella, A., Boucher, O., Shine, K.P., Stettler, M., Tanaka, K., Teoh, R., Bellouin, N., 2024. The importance of an informed choice of co_2-equivalence metrics for contrail avoidance. EGUsphere 2024, 1–24.

Bosilovich, M., Lucchesi, R., Suarez, M., 2016. Merra-2: File Specification. Gmao Office Note No. 9 (Version 1.1), p. 73 available from: http://gmao.gsfc.nasa.gov/pubs/office_notes.

Burkhardt, U., Bock, L., Bier, A., 2018. Mitigating the contrail cirrus climate impact by reducing aircraft soot number emissions. npj Clim. Atmosph. Sci. 1 (1), 37.

Dischl, R., Kaufmann, S., Voigt, C., 2022. Regional and seasonal dependence of the potential contrail cover and the potential contrail cirrus cover over europe. Aerospace 9 (9).

Dyroff, C., Zahn, A., Christner, E., Forbes, R., Tompkins, A.M., van Velthoven, P.F.J., 2015. Comparison of ecmwf analysis and forecast humidity data with caribic upper troposphere and lower stratosphere observations. Q. J. R. Meteorol. Soc. 141 (688), 833–844.

European Comission, 2024. The european green deal. https://commission.europa.eu/strategy-and-policy/priorities-2019-2024/european-green-deal_en, 2024-03-06.

Frömming, C., Grewe, V., Brinkop, S., Jöckel, P., Haslerud, A.S., Rosanka, S., van Manen, J., Matthes, S., 2021. Influence of weather situation on non-co_2 aviation climate effects: the react4c climate change functions. Atmos. Chem. Phys. 21, 127–141.

Gierens, K., 2021. Theory of contrail formation for fuel cells. Aerospace 8 (6), 164.

Gierens, K., Matthes, S., Rohs, S., 2020. How well can persistent contrails Be predicted? Aerospace 7 (12), 169.

Global Modeling and Assimilation Office (GMAO), 2015. MERRA-2 inst3_3d_asm_Np: 3d,3-Hourly,Instantaneous,Pressure-Level,Assimilation,Assimilated Meteorological Fields V5.12.4, Greenbelt, MD, USA, Goddard Earth Sciences Data and Information Services Center (GES DISC). https://doi.org/10.5067/QBZ6MG944HW0, 09.11.2022.

Grewe, V., Bock, L., Burkhardt, U., Dahlmann, K., Gierens, K., Hüttenhofer, L., Unterstrasser, S., Rao, A.G., Bhat, A., Yin, F., Reichel, T.G., Paschereit, O., Levy 12, Y., 2017. Assessing the climate impact of the ahead multi-fuel blended wing body. Meteorol. Z. 26 (6), 711–725.

Hersbach, H., Bell, B., Berrisford, P., Biavati, G., Horányi, A., Muñoz Sabater, J., Nicolas, J., Peubey, C., Radu, R., Rozum, I., Schepers, D., Simmons, A., Soci, C., Dee, D., Thépaut, J.-N., 2018. ERA5 hourly data on pressure levels from 1979 to present. Copernicus Clim. Change Serv. (C3S) Clim. Data Store (CDS).

Hofer, S., Gierens, K., Rohs, S., 2024a. Contrail formation and persistence conditions for alternative fuels. Meteorol. Z.

Hofer, S.M., Gierens, K.M., Rohs, S., 2024b. How well can persistent contrails be predicted? an update. Atmos. Chem. Phys. 24, 7911–7925.

ICAO, 2018. Icao gis aeronautical data: icao traffic flow 2018. https://gis.icao.int/portal/home/. (Accessed 19 September 2024).

ICAO, 2021. Icao report: the world of air transport in 2021. https://www.icao.int/sustainability/worldofairtransport/pages/the-world-of-air-transport-in-2021.aspx. (Accessed 14 December 2023). https://www.icao.int/annual-report-2021/documents/20230320_final_table_en.pdf.

Jiang, W.P., Qingfeng, L., 2021. Introduction to Fuel Cells, first ed. Springer Singapore, Singapore.

Kaufmann, S., Voigt, C., Heller, R., Brown, T.R., Krämer, M., Rolf, C., Zöger, M., Giez, A., Buchholz, B., Ebert, V., Thornberry, T., Schumann, U., 2018. Intercomparison of midlatitude tropospheric and lower-stratospheric water vapor measurements and comparison to ECMWF humidity data. Atmos. Chem. Phys. 18 (22), 16729–16745.

Koop, T., Luo, B., Tsias, A., Peter, T., 2000. Water activity as the determinant for homogeneous ice nucleation in aqueous solutions. Nature 406 (6796), 611–614.

Lee, D., Fahey, D., Skowron, A., Allen, M., Burkhardt, U., Chen, Q., Doherty, S., Freeman, S., Forster, P., Fuglestvedt, J., Gettelman, A., De León, R., Lim, L., Lund, M., Millar, R., Owen, B., Penner, J., Pitari, G., Prather, M., Sausen, R., Wilcox, L., 2021. The contribution of global aviation to anthropogenic climate forcing for 2000 to 2018. Atmos. Environ. 244, 117834.

Li, Y., Mahnke, C., Rohs, S., Bundke, U., Spelten, N., Dekoutsidis, G., Groß, S., Voigt, C., Schumann, U., Petzold, A., Krämer, M., 2023. Upper-tropospheric slightly ice-subsaturated regions: frequency of occurrence and statistical evidence for the appearance of contrail cirrus. Atmos. Chem. Phys. 23 (3), 2251–2271.

Marquart, S., Ponater, M., Ström, L., Gierens, K., 2005. An upgraded estimate of the radiative forcing of cryoplane contrails. Meteorol. Z. 14, 573–582.

Ponater, M., Pechtl, S., Sausen, R., Schumann, U., Hüttig, G., 2006. Potential of the cryoplane technology to reduce aircraft climate impact: a state-of-the-art assessment. Atmos. Environ. 40 (36), 6928–6944.

Sausen, R., G, K., M, P., U, S., 1998. A diagnostic study of the global distribution of contrails part i: present day climate. Theor. Appl. Climatol. 61 (11), 9151–9172.

Schumann, U., 1996. On conditions for contrail formation from aircraft exhausts. Meteorol. Z. 5 (1), 4–23.

Schumann, U., 2012. A contrail cirrus prediction model. Geosci. Model Dev. (GMD) 5 (3), 543–580.

Schumann, U., Penner, J.E., Chen, Y., Zhou, C., Graf, K., 2015. Dehydration effects from contrails in a coupled contrail–climate model. Atmos. Chem. Phys. 15 (19), 11179–11199.

Teoh, R., Engberg, Z., Schumann, U., Voigt, C., Shapiro, M., Rohs, S., Stettler, M., 2024. Global aviation contrail climate effects from 2019 to 2021. Atmos. Chem. Phys. 24, 6071–6093.

Teoh, R., Schumann, U., Gryspeerdt, E., Shapiro, M., Molloy, J., Koudis, G., Voigt, C., Stettler, M.E.J., 2022a. Aviation contrail climate effects in the north atlantic from 2016 to 2021. Atmos. Chem. Phys. 22 (16), 10919–10935.

Teoh, R., Schumann, U., Voigt, C., Schripp, T., Shapiro, M., Engberg, Z., Molloy, J., Koudis, G., Stettler, M.E.J., 2022b. Targeted use of sustainable aviation fuel to maximize climate benefits. Environ. Sci. Technol. 56 (23), 17246–17255 pMID: 36394538.

Unterstrasser, S., 2016. Properties of young contrails – a parametrisation based on large-eddy simulations. Atmos. Chem. Phys. 16 (4), 2059–2082.

Voigt, C., Kleine, J., Sauer, D., Moore, R., Bräuer, T., Le Clercq, P., Kaufmann, S., Scheibe, M., Jurkat-Witschas, T., Aigner, M., Bauder, U., Boose, Y., Borrmann, S., Crosbie, E., Diskin, G.S., DiGangi, J., Hahn, V., Heckl, C., Huber, F., Nowak, J.B., Rapp, M., Rauch, B., Robinson, C., Schripp, T., Shook, M., Winstead, E., Ziemba, L., Schlager, H., Anderson, B.E., 2021. Cleaner burning aviation fuels can reduce contrail cloudiness. Commun. Earth Environ. 2 (1), 114.

Warwick, N.J., Archibald, A.T., Griffiths, P.T., Keeble, J., O'Connor, F.M., Pyle, J.A., Shine, K.P., 2023. Atmospheric composition and climate impacts of a future hydrogen economy. Atmos. Chem. Phys. 23 (20), 13451–13467. URL. https://acp.copernicus.org/articles/23/13451/2023/.

Wolf, K., Bellouin, N., Boucher, O., Rohs, S., Li, Y., 2023. Correction of Temperature and Relative Humidity Biases in Era5 by Bivariate Quantile Mapping: Implications for Contrail Classification, vol. 2023. EGUsphere, pp. 1–38.